

PCCP

Accepted Manuscript



This is an *Accepted Manuscript*, which has been through the Royal Society of Chemistry peer review process and has been accepted for publication.

Accepted Manuscripts are published online shortly after acceptance, before technical editing, formatting and proof reading. Using this free service, authors can make their results available to the community, in citable form, before we publish the edited article. We will replace this *Accepted Manuscript* with the edited and formatted *Advance Article* as soon as it is available.

You can find more information about *Accepted Manuscripts* in the [Information for Authors](#).

Please note that technical editing may introduce minor changes to the text and/or graphics, which may alter content. The journal's standard [Terms & Conditions](#) and the [Ethical guidelines](#) still apply. In no event shall the Royal Society of Chemistry be held responsible for any errors or omissions in this *Accepted Manuscript* or any consequences arising from the use of any information it contains.

www.rsc.org/

Simultaneous enhancement of magnetic and ferroelectric properties in Dy and Cr co-doped BiFeO₃ nanoparticles

Weiwei Mao^{a,b}, Xingfu Wang^{a,b}, Liang Chu^b, Yiyi Zhu^a, Qi Wang^a, Jian Zhang^a, Jianping Yang^b, Xing'ao Li^{a*} and Wei Huang^{a,c*}

Multiferroic BiFeO₃ (BFO), Bi_{0.95}Dy_{0.05}FeO₃, and Bi_{0.95}Dy_{0.05}Fe_{0.95}Cr_{0.05}O₃ samples were successfully synthesized by a carbon microsphere-assisted sol-gel (CSG) method. X-ray diffraction analysis confirmed a lattice distortion from rhombohedral structure to tetragonal structure by doping Dy and Cr in BFO. The morphology of BFO and doped-BFO can be effectively controlled to form nanoparticles, due to the nucleation sites of carbon microspheres. The co-doping of Dy and Cr in BFO has significant effect on improvement magnetic properties with the remnant magnetization of 0.557 emu/g, due to the structural phase transition, size effects, and the strong ferromagnetic interaction between Fe³⁺-O-Cr³⁺ ions by Cr substitution. Meanwhile, the doping of Dy into BFO effectively reduced the leakage current and enhanced the ferroelectric properties. The simultaneous enhancement of magnetic and ferroelectric properties shows the great potential application of Dy and Cr co-doped BFO in the future multifunctional devices.

1. Introduction

Multiferroics capture great attention for the potential application in multifunctional devices, which simultaneous possess ferroic properties, such as ferroelectricity, ferromagnetism, and ferroelasticity, coupled with electric, magnetic, and structural order parameters.¹⁻³ So far, several single-phase multiferroics have been developed, such as YMnO₃, BiMnO₃, DyMnO₃, BiFeO₃ (BFO).⁴⁻⁷ Of those, BFO is known to be the only one with simultaneous ferroelectric (T_c~1103 K) and G-type antiferromagnetic (TN~ 643 K) orderings at room temperature.⁸ The unique multiferroic behaviour lets BFO to be an ideal candidate for most important multifunctional applications.⁹⁻¹¹ However, the bulk BFO is characterized by some inherent problems including high leakage current, persistent formation of secondary phases, and weak ferromagnetism. The combined action of exchange and spin-orbit interactions produce spin canting away from perfect antiferromagnetic ordering, and resulting in a small magnetic moment. But the moment direction would rotate and superimpose a spiral-modulated spin structure with a wavelength of 62 nm, generating a vanishing magnetization in the BFO.¹²

Based on the hypothesis of Spaldin, the ferroelectricity and magnetism of BFO mainly result from lone pair electrons of Bi³⁺ ions and the magnetism of Fe³⁺ ions, respectively.^{13, 14} Hence, several research groups have tried A-site substitution by selected trivalent rare-earth and divalent ions¹⁵⁻¹⁸ or B-site substitution by transition metal ions¹⁹⁻²¹ in order to improve the multiferroic properties. It was observed that the Dy-doped

BFO thin films significantly enhanced ferroelectric and fatigue properties because of the reduction of oxygen vacancies.²² In addition, Dy doping was demonstrated to be a very effective method for inducing a weakly ferromagnetic state in the ferroelectric R3c phase of BFO in the absence of an external magnetic field.²³ Moreover, it has been reported that the Cr³⁺ substitution on Fe-site can enhance the magnetization due to strong ferromagnetic interaction between Fe³⁺ and Cr³⁺.²⁴⁻²⁶ However, there has been no reports of Dy and Cr co-doping, which may both improve ferroelectric and magnetic properties in BFO system.

Herein we present a carbon microsphere-assisted sol-gel (CSG) method to synthesize the Dy and Cr co-doped BFO nanoparticles, which exhibit simultaneously enhanced magnetic and ferroelectric properties comparing with the pure BFO. The origins of the improved magnetic and ferroelectric properties are detailedly discussed in this work. Meanwhile, we also present the analysis of the influence on the introduction of carbon microspheres, which play a role in reducing the grain sizes and enhancing magnetic properties. Thereby, it may be an effective way to improve the magnetic and ferroelectric properties via co-doping Dy and Cr into BFO prepared by CSG method.

2. Experimental

2.1. Preparations of carbon microspheres

Carbon microspheres were prepared by a hydrothermal method.²⁷ Glucose (6.0 g) was dissolved in deionized water (40

ml) with the aid of ultrasonication. The solution was transferred into a Teflon-lined stainless steel autoclave with 50 mL inner, and then loaded into an oven at 180 °C for reaction for 4 h. After the reaction, the obtained products were harvested, and washed with deionized water for several times via centrifugation. Finally, the as-prepared carbon microspheres were dried at 70 °C for two days.

2.2. Preparations of BFO



Fig. 1. Schematics for the synthesis of the samples via a carbon microsphere-assisted sol-gel method

Polycrystalline samples of pure BFO (BFO-C), $\text{Bi}_{0.95}\text{Dy}_{0.05}\text{FeO}_3$ (Dy5-C), and $\text{Bi}_{0.95}\text{Dy}_{0.05}\text{Fe}_{0.95}\text{Cr}_{0.05}\text{O}_3$ (Dy5Cr5-C) were synthesized via a carbon microsphere-assisted sol-gel method. A schematic illustration of the preparation was shown in Fig. 1. Appropriate proportions of Bi_2O_3 , $\text{Fe}(\text{NO}_3)_3 \cdot 9\text{H}_2\text{O}$, Dy_2O_3 and $\text{Cr}(\text{NO}_3)_3 \cdot 9\text{H}_2\text{O}$ were used as precursor materials, which were dissolved in dilute nitric acid with a chelating agent of tartaric acid. Carbon microspheres (0.08 g) were dispersed in 10 mL distilled water with the aid of ultrasonication for 1 h. For assisting by carbon microspheres, the suspension was added drop-by-drop into the above precursor solution of BFO and vigorously stirred for 12 h. Then, the mixed suspension was dried at 70 °C for 24 h and calcined at 600 °C for 2 h. To make a comparison, BFO (BFO), $\text{Bi}_{0.95}\text{Dy}_{0.05}\text{FeO}_3$ (Dy5), and $\text{Bi}_{0.95}\text{Dy}_{0.05}\text{Fe}_{0.95}\text{Cr}_{0.05}\text{O}_3$ (Dy5Cr5) were also synthesized by

conventional sol-gel (SG) method, as reported in our earlier paper.²⁸

2.3. Characterization

The structure and phase purity of the samples were characterized by X-ray diffraction (XRD) using $\text{Cu-K}\alpha$ radiation at room temperature. The morphology and local element occupancy were examined using scanning electron microscopy (SEM, JEOL-6380LV Japan) and energy dispersive X-ray spectroscopy (EDS, HORIBA EMAX Energy EX-250). Transmission electron microscopy (TEM) imaging and grain size were performed on a JEOL JEM-2100 microscope, by depositing a drop of samples dispersion onto 300 mesh Cu grids coated with a carbon layer. The ferroelectric hysteresis loops (P - E) and leakage current density-electric field (J - E) curves were measured using Radiant precision materials analyzer with each powder sample pressed into thin piece under a pressure of 20 MPa having an area around 0.2 cm^2 and a thickness around 0.08 cm. Ag electrodes were coated on both sides. The magnetization hysteresis (M - H) loops were evaluated at room temperature up to a field of 50 kOe using a vibrating sample magnetometer (VSM).

3. Results and discussion

The XRD patterns of all the samples are shown in Fig. 2 (a). All the diffraction peaks associated with the pure BFO nanoparticles are well matched with the rhombohedral structure (JCPDS file No. 71-2494). Comparing the two methods, there is no difference in XRD patterns of the samples prepared by different methods. It suggests that the presence of carbon microspheres did not affect the synthesis of BFO and doped BFO. The role of carbon microspheres additive in decreasing the average grain size of BFO can be explained as follows. There are small amounts of impurity phases $\text{Bi}_2\text{Fe}_4\text{O}_9$ for BFO-C, Dy5Cr5 and Dy5Cr5-C, as marked by "*" in Fig. 2 (a). The absence of the diffraction peaks of the oxides of Dy or Cr implies that substitution did not trigger the formation of the impurity phase, thereby means that Dy and Cr ions have doped

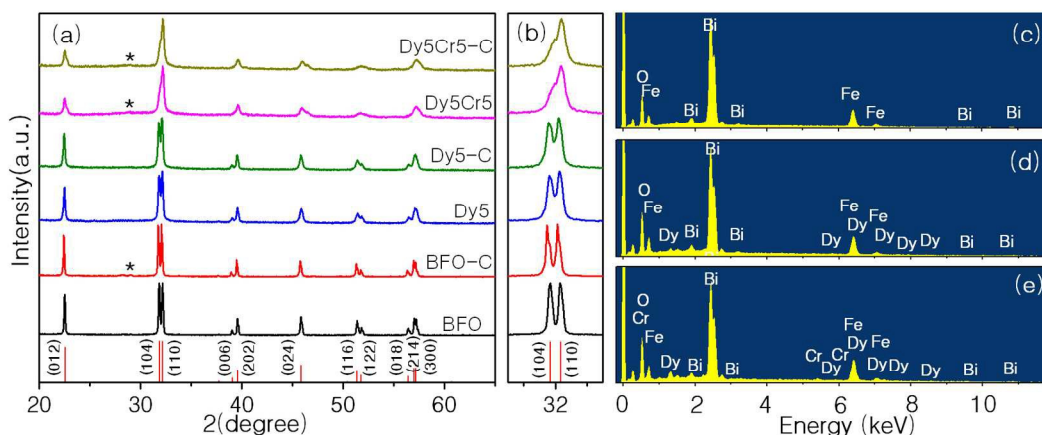


Fig. 2. (a) X-ray diffraction patterns of all the samples at room temperature. (b) Enlarged view of the diffraction peaks (104) and (110). Typical EDS patterns of (c) BFO-C, (d) Dy5-C and (e) Dy5Cr5-C.

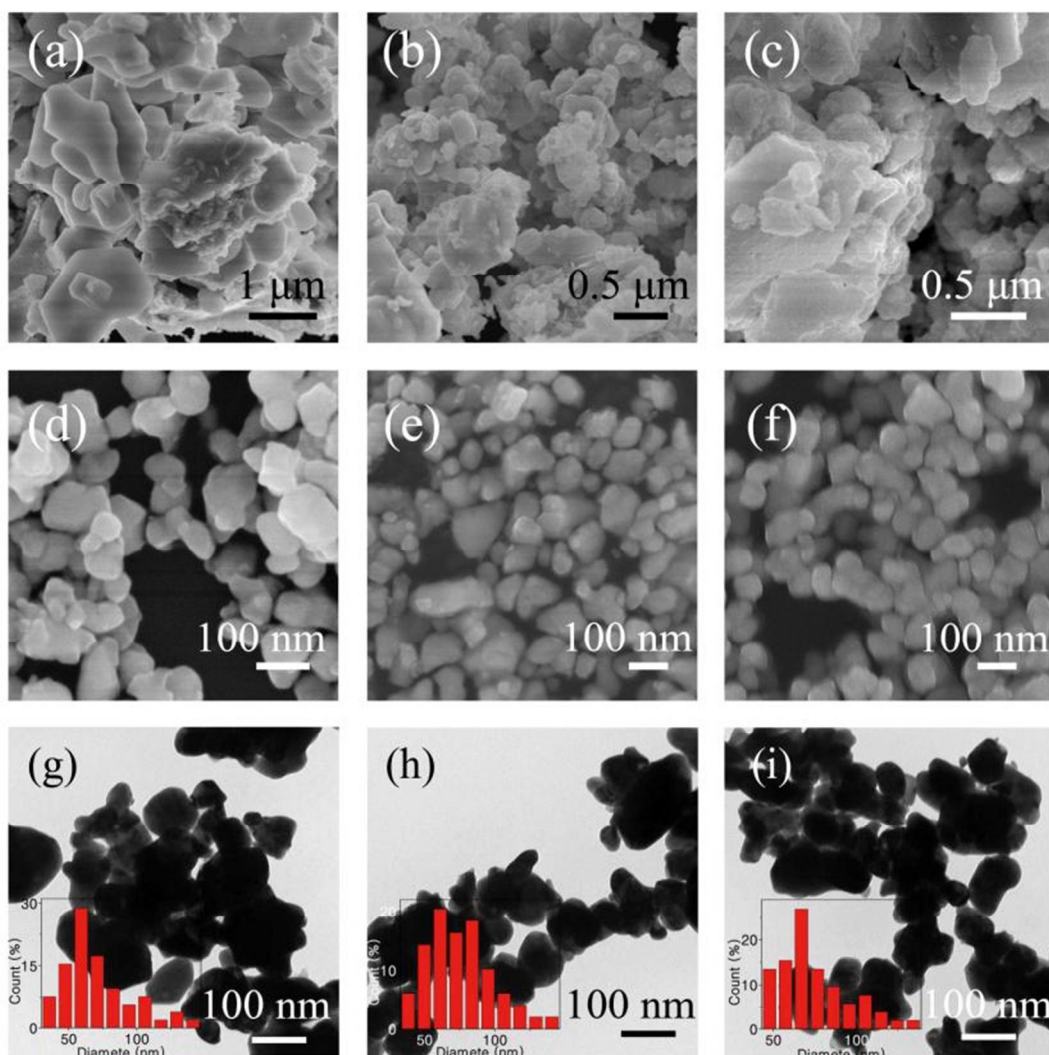


Fig. 3. SEM images for (a) BFO, (b) Dy5, (c) Dy5Cr5, (d) BFO-C, (e) Dy5-C, (f) Dy5Cr5-C. TEM images for (g) BFO-C, (h) Dy5-C, (i) Dy5Cr5-C. Insets in (g-i) show the particle size distribution of BFO-C, Dy5-C and Dy5Cr5-C, respectively.

into BFO successfully. The enlarged version of the XRD patterns in the range of 2θ 31° - 34° is displayed in Fig. 2 (b), which reveals a evolution of the (104) and (110) diffraction peaks. The two peaks are clearly separated in BFO (BFO-C), then show a trend to coalescence in Dy5 (Dy5-C) samples. After co-doping with Dy and Cr, the doubly split peaks merge to form one peak in Dy5Cr5 (Dy5Cr5-C). This phenomena indicates that substitution induces structural distortion which can be attributed to the Dy^{3+} ion with a smaller ionic radius than Bi^{3+} ion and the Cr^{3+} ion with a smaller ionic radius than Fe^{3+} ion.^{29,30} Furthermore, the single Dy-doping concentration of 5 mol% only leads to some kind of structural distortion. While co-doping can cause a lattice distortion from rhombohedral structure to tetragonal structure. Similar behaviour has also been observed in other reports.³¹⁻³³ The elemental analysis was carried out using the EDS analysis. Typical EDS patterns of BFO-C, Dy5-C and Dy5Cr5-C have been shown in Fig. 2 (c)-(e). The chemical composition of BFO-C

agrees with the nominal one 1:1:3 approximately. Besides the obvious signals for O, Bi, and Fe, the EDS spectra show weak signal of Dy in Dy5-C and Dy/Cr in Dy5Cr5-C. The measured quantitative values demonstrate the atomic percentage of 16.95% Bi, 1.08% Dy for Dy5-C and 16.53% Bi, 1.30% Dy, 17.31% Fe, 1.12% Cr for Dy5Cr5-C, respectively. According to the above results, it is evident that Dy and Cr ions have been effectively incorporated into the host material.

The morphology of the as-synthesized samples was observed by SEM. Fig. 3 (a-c) shows the typical surface SEM images of the conventional SG processed samples. If there were no carbon microspheres, the morphologies were random without any regular particles, and the grain sizes were nearly reached microscale. It was surprised that by the assistance of carbon microspheres, the grain sizes reduced from microscale to nanoscale, as shown in Fig. 3 (d-f). Additional support was obtained by TEM characterization. Fig. 3 (g-i) show the typical TEM images of BFO-C, Dy5-C and Dy5Cr5-C. The histograms of

particle size distribution are shown in inset of Fig. 3 (g-i) getting from TEM images. It can be measured that the average grain sizes of BFO-C, Dy5-C and Dy5Cr5-C are 71.14 nm, 68.26 nm and 69.31 nm, respectively. It was concluded that the carbon microspheres had a significant impact on the formation of uniform BFO particles. It is well known that the agglomeration is taking place due to high surface energy of the nanoparticles. In our experiment, carbon microspheres became the nucleation sites of BFO when they were added into BFO solution, which was illustrated in Fig. 1. BFO nanoparticles are nucleated in the solution, and then they are adsorbed onto the carbon microspheres surface because surface energy of carbon microspheres is lower than that of BFO. After calcined in air to remove the carbon microspheres, the BFO nanoparticles were obtained with effectively reduced grain size and homogeneous microstructures.

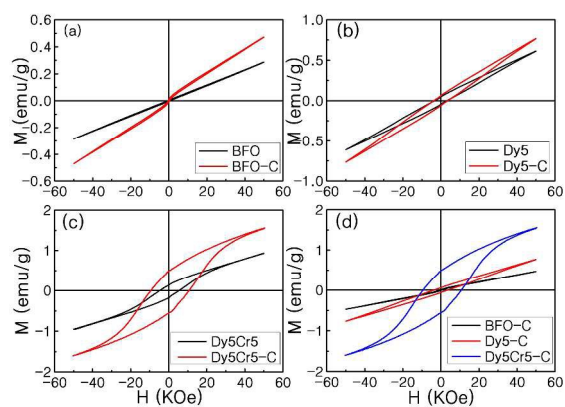


Fig. 4. Room temperature magnetic hysteresis loops for (a) BFO and BFO-C, (b) Dy5 and Dy5-C, (c) Dy5Cr5 and Dy5Cr5-C, (d) BFO-C, Dy5-C and Dy5Cr5-C.

Fig. 4 (a)-(c) shows the comparison of the magnetic hysteresis (M - H) loops for the conventional SG-prepared and CSG-prepared samples at room temperature with a maximum applied field of 50 kOe. Table 1 summarizes the values of remnant magnetization (M_r), coercive field (H_c) and Maximum magnetization (M_s) at 50 kOe, which clearly demonstrate the enhanced magnetic parameters of the samples prepared by CSG method. The enhancement in ferromagnetism can be possibly attributed to the present of $\text{Bi}_2\text{Fe}_4\text{O}_9$, because of the weak ferromagnetic properties in $\text{Bi}_2\text{Fe}_4\text{O}_9$ nanoparticles.^{34, 35} In addition, the enhanced magnetic properties may be attributed to the size effect of the nanoparticles. When the dimensions of BFO are decreased to the nanoscale, they start to exhibit a variety of new physical phenomena, such as weak ferromagnetism.³⁶⁻³⁸ In accordance with the Néel theory, the magnetization in antiferromagnetic material can be described as comprising two spin sublattices with ferromagnetic interactions within one sublattice and antiferromagnetic interactions between sublattices.³⁹ These materials should exhibit superparamagnetism and weak ferromagnetism, which was attributed to the permanent magnetic moment to incomplete spin compensation between the two spin sublattices. This incomplete spin compensation gives rise to a

measurable magnetic moment in case of small antiferromagnetic systems as the antiferromagnetic ordering gets interrupted at the surface of the particle.^{36, 37} As the surface to volume ratio becomes large with decreasing particle size in nanoparticles, the uncompensated spins at the surface contribute substantially towards the enhancement of particles' overall magnetization.

Table 1 Magnetic parameters at room temperature

	Maximum magnetization (emu/g)	Remnant magnetization (emu/g)	Coercive field (kOe)
BFO	0.286	0.0033	0.622
BFO-C	0.471	0.0065	0.313
Dy5	0.611	0.0438	3.283
Dy5-C	0.765	0.0580	3.283
Dy5Cr5	0.927	0.174	4.731
Dy5Cr5-C	1.542	0.557	9.348
Dy10-C	1.373	0.243	8.242

Substitution is known to be an effective way to enhance the ferromagnetic properties of BFO via varying the electronic and crystalline structure. To investigate the effect of substitution on the ferromagnetic properties, the field-dependent magnetization of the three CSG-prepared samples measured at room temperature are shown in Fig. 4 (d). The M - H curves indicate that the ferromagnetic properties of doped samples are much more enhanced than that of BFO-C. For pure BFO-C, magnetization increases linearly with increase of magnetic field and the maximum magnetization (M_s) at the maximum applied field of 50 kOe corresponds to 0.471 emu/g, which suggests that pure BFO is antiferromagnetic.⁴⁰ Compared with BFO-C, clear hysteresis loops are observed in the Dy5-C and Dy5Cr5-C samples. There is a slight increase in the maximum magnetization of the individual substitution of Dy element ($M_s \sim 0.765$ emu/g) compared to BFO-C. The highest value of M_s (~ 1.542 emu/g), M_r (~ 0.557 emu/g) and H_c (~ 9.348 kOe) occurs in the double doped Dy5Cr5-C samples. The origin of weak ferromagnetism in BFO is the spin of Fe^{3+} , which is responsible for G-type antiferromagnetic ordering modified by a long-range modulation of the cycloidal spiral.^{12, 41} This cycloidal structure results in the disappearance of the macroscopic magnetization. So the enhanced magnetization in Dy5-C and Dy5Cr5-C could be due to the structural distortion, based on the structural analysis of XRD data. The structural distortion destroyed the spiral spin modulation in BFO, so that the latent magnetization locked within the cycloid might be released. In Dy5-C sample, individual substitution of Dy can only suppress but cannot destroy the spin cycloid structure completely, leading to limited increase of magnetization. However, the Dy and Cr co-doping induced a structural phase transition wherein the spin cycloid might be destructed.⁴² Therefore, significant increased magnetization is observed in Dy5Cr5-C sample.

In order to further analyze and understand the role of Cr-doping on the ferromagnetic properties, we prepared $\text{Bi}_{0.90}\text{Dy}_{0.10}\text{FeO}_3$ (Dy10-C) nanoparticles by the same method.

The XRD patterns of Dy5Cr5-C and Dy10-C are shown in Fig. 5 (a). All the diffraction peaks are almost same for the two samples. The room temperature $M-H$ loops of Dy5Cr5-C and Dy10-C are shown in Fig. 5 (b). The M_s at the maximum applied field of 50 kOe and the M_r in the Dy10-C are 1.37 emu/g and 0.243 emu/g, respectively. Dy5Cr5-C exhibits the enhanced value of M_r to 0.557 emu/g, which is almost twice than that for Dy10-C. In principle, M_r is due to weak ferromagnetic attributed to the canting which is caused by the Dzyaloshinsky-Moriya interaction interactions in multiferroic perovskites.⁴³ Due to the paramagnetic contribution from Dy ions, the $M-H$ loops do not exhibit any saturation for Dy10-C.²⁹ In contrast to this case, the room temperature field-dependent magnetization of Dy5Cr5-C begins to exhibit some saturation of the magnetization in the highest magnetic fields. By taking into account of the similar crystal structure with the aforementioned XRD data, the further increased magnetization of Dy5Cr5-C might be due to the substitution of Fe^{3+} by Cr^{3+} . As is known to all, BFO presents a weak magnetization because of $\text{Fe}^{3+}\text{-O-Fe}^{3+}$ antiferromagnetic exchange interaction. When Cr^{3+} ions occupy Fe-sites, the ferromagnetic interaction between $\text{Fe}^{3+}\text{-O-Cr}^{3+}$ ions appears, which playing the key role for the enhancement of the magnetization, especially the larger M_r and H_c . Koval et al. reported that the M_r was about 0.21 emu/g for the $\text{Bi}_{0.9}\text{Dy}_{0.1}\text{FeO}_3$ ceramic synthesized by solid-state reaction method.²³ Das et al. evaluated the magnetic properties of Cr-doped BFO nanotubes which exhibited weak ferromagnetic behaviour with M_r and H_c of 0.00054 emu/g and 0.023 kOe, respectively.⁴⁴ Dutta et al. synthesized $\text{BiFe}_{0.9}\text{Cr}_{0.1}\text{O}_3$ and $\text{BiFe}_{0.9}\text{Mn}_{0.1}\text{O}_3$ nanorods using a sonochemical technique. The obtained M_r and H_c were around 0.05 emu/g and 0.35 kOe for $\text{BiFe}_{0.9}\text{Cr}_{0.1}\text{O}_3$, 0.02 emu/g and 0.57 kOe for $\text{BiFe}_{0.9}\text{Mn}_{0.1}\text{O}_3$, respectively.³⁶ Apparently, M_r and H_c of Dy5Cr5-C are higher than those of single doped Dy or Cr doped BFO in the earlier works. Furthermore, the values in the present work are well comparable with those previous values of BFO doped by Pr, Ho, Eu and Sr elements.⁴⁵⁻⁴⁷ The promising magnetic properties achieved in the present Dy5Cr5-C samples could be associated with the size effect, the structural phase transition and the ferromagnetic interaction between $\text{Fe}^{3+}\text{-O-Cr}^{3+}$ ions.

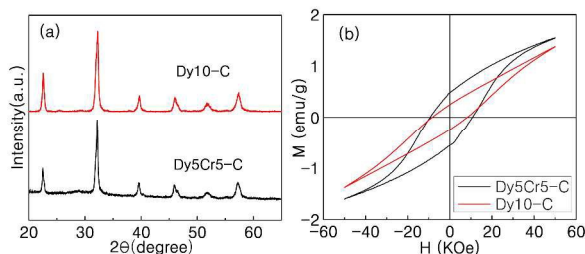


Fig. 5. (a) X-ray diffraction patterns of Dy5Cr5-C and Dy10-C, (b) Magnetic hysteresis loops for Dy5Cr5-C and Dy10-C.

Fig. 6 (a) shows the leakage current density (J) as functions of the applied electric field (E) of BFO-C, Dy5-C and Dy5Cr5-C measured at room temperature. It is clear that all the $J-E$ curves have good symmetry under positive and negative electric fields. For the pure BFO-C, the leakage current density is $4.19 \times 10^{-5} \text{ A/cm}^2$ at an applied electric field of 20 kV/cm. At the same applied electric field, the leakage current density of Dy5-C is $4.17 \times 10^{-6} \text{ A/cm}^2$, which is about one order of magnitude lower than that of BFO-C. It can be also obtained from $J-E$ data that Cr doping in Dy5-C does not lead to obvious change. This clearly reveals that the leakage current density can be effectively reduced by the substitution of Dy element. As known to all, the large leakage current density in BFO mainly results from charge defects such as oxygen vacancies. The oxygen vacancies arise due to Bi deficiency of the volatile at high temperature.⁴⁸ Dy substitution as other rare earth substituents in Bi site of BFO can suppress the formation of oxygen vacancies by controlling volatility of Bi atoms and stabilizing the oxygen octahedron.¹⁶ So the decrease of leakage current density in the two doped samples is mainly due to the reduction in the concentration of oxygen vacancies caused by Dy doping.

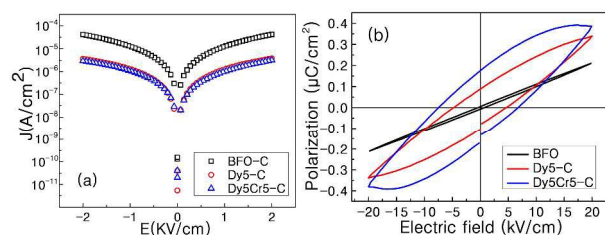


Fig. 6. (a) The leakage current density-electric field behaviours for BFO-C, Dy5-C and Dy5Cr5-C samples. (b) Polarization hysteresis loops of BFO-C, Dy5-C and Dy5Cr5-C samples.

To ascertain the ferroelectric behaviour of BFO-C, Dy5-C and Dy5Cr5-C nanoparticles, the polarization hysteresis ($P-E$) loops were measured under an applied electric field (E) of about 20 kV/cm, which is shown in Fig. 6 (b). It is clearly observed that all the samples show unsaturated $P-E$ curves, which revealing high leakage current. As known, the high leakage current in BFO mainly originated from charge defects such as bismuth vacancies or oxygen vacancies. The oxygen vacancies arise due to Bi deficiency with its highly volatile nature and the valence fluctuations of Fe.⁴⁸ For the pure BFO-C, a linear $P-E$ loops with weak remnant polarization $2Pr$ ($0.0146 \mu\text{C/cm}^2$) were observed. Compared with BFO-C, a significant improvement of the ferroelectric properties can be observed of the substitution produces. The $2Pr$ and the coercive electric field (E_c) of the Dy doped BFO are $0.210 \mu\text{C/cm}^2$ and 4.807 kV/cm , respectively. Better ferroelectric properties are exhibited in the Dy5Cr5-C, and both $2Pr$ and E_c increased to $0.370 \mu\text{C/cm}^2$ and 7.511 kV/cm , respectively. As confirmed by $J-E$ curves, Dy substitution can suppress the oxygen vacancies, therefore decrease leakage current density and enhance the ferroelectric behaviour of BFO. Furthermore, the origin of ferroelectricity in BFO is generally due to Bi^{3+} ($6s^2$) lone pair electron.⁴⁹ The stereochemical activity of lone pair

will be enhanced by the structure transition as a result of Dy and Cr codoped in BFO indicated by XRD patterns.⁵⁰ So the structure transition might be another reason for the better ferroelectric properties of the Dy5Cr5-C nanoparticles.

4. Conclusion

In summary, an innovative approach for preparing Dy and Cr co-doped BFO nanoparticles by a carbon microsphere-assisted sol-gel (CSG) method is presented in this paper. The XRD results show the formation of impurity phases by the addition of carbon microspheres, and a phase transition from rhombohedral to tetragonal structure by co-doping Dy-Cr into BFO. Compared with the conventional SG-prepared samples, the grain sizes of CSG-prepared samples reached to nanoscale with the average sizes of 71.14 nm for BFO-C and 69.31 nm for Dy5Cr5-C. The Dy5Cr5-C nanoparticles exhibit the greatly enhanced magnetic and ferroelectric properties. All these results suggest that the CSG method and the co-doping of Dy and Cr in BFO are the effective way to improve magnetic and ferroelectric properties, which are essential for practical applications.

Acknowledgements

We acknowledge the financial support from the Ministry of Education of China (No. IRT1148), the National Synergistic Innovation Center for Advanced Materials (SICAM), the Natural Science Foundation of Jiangsu Province, China (BM2012010), the Project Funded by the Priority Academic Program Development of Jiangsu Higher Education Institutions (PAPD, YX03001), Science and Technology Innovation on Training Program (STITP, SZDG2014018) and the National Natural Science Foundation of China (51172110, 51372119, 61377019, 61136003, 51173081), College Postgraduate Research and Innovation Project of Jiangsu Province (KYLX_0794, KYLX15_0848), the Natural Science Foundation of Scientific and Technological Department of Jiangsu Province (KZ0070715050), the Seed Project Funded by Introducing Talent of NJUPT (XK0070915022), the Natural Science Foundation of NJUPT (NY214129, NY214130, NY214181).

Notes and references

^a Key Laboratory for Organic Electronics & Information Displays (KLOEID), Institute of Advanced Materials (IAM), School of Materials Science and Engineering (SMSE), Nanjing University of Posts and Telecommunications (NUPT), Nanjing 210023, P R China. Tel: +86-02585866362; E-mail: lxahbmy@126.com; Tel: +86-02585866533; E-mail: iamwhuang@njupt.edu.cn

^b College of Science, Information Physics Research Center, Advanced Energy Technology Center, Nanjing University of Posts and Telecommunications (NUPT), Nanjing 210023, P R China.

^c Key Laboratory of Flexible Electronics (KLOFE) & Institute of Advanced Materials (IAM), National Synergistic Innovation Center for

Advanced Materials (SICAM), Nanjing Tech University (NanjingTech), 30 South Puzhu Road, Nanjing 211816, China.

1. W. Eerenstein, N. D. Mathur and J. F. Scott, *Nature*, 2006, **442**, 759-765.
2. S. W. Cheong and M. Mostovoy, *Nature materials*, 2007, **6**, 13-20.
3. J. Ma, J. Hu, Z. Li and C. W. Nan, *Advanced materials*, 2011, **23**, 1062-1087.
4. T. Ahmad, I. H. Lone and M. Ubaidullah, *RSC Advances*, 2015, **5**, 58065-58071.
5. B. Sun, C. M. Li, *Physical Chemistry Chemical Physics*, 2015, **17**, 6718-6721.
6. J. Magesh, P. Murugavel, R. V. K. Mangalam, K. Singh, C. Simon and W. Prellier, *Journal of Applied Physics*, 2015, **118**, 074102.
7. B. Sun, L. J. Wei, H. W. Li and P. Chen, *Journal of Materials Chemistry C*, 2014, **2**, 7547-7551.
8. J. Wang, J. B. Neaton, H. Zheng, V. Nagarajan, S. B. Ogale, B. Liu, D. Viehland, V. Vaithyanathan, D. G. Schlom, U. V. Waghmare, N. A. Spaldin, K. M. Rabe, M. Wuttig and R. Ramesh, *Science*, 2003, **299**, 1719-1722.
9. B. Sun, Y. H. Liu, W. X. Zhao and P. Chen, *RSC Advances*, 2015, **5**, 13513-13518.
10. R. Guo, L. You, Y. Zhou, Z. S. Lim, X. Zou, L. Chen, R. Ramesh and J. Wang, *Nature communications*, 2013, **4**, 1990.
11. X. F. Wang, W. W. Mao, J. Zhang, Y. M. Han, C. Y. Quan, Q. X. Zhang, T. Yang, J. P. Yang, X. A. Li and W. Huang, *Journal of colloid and interface science*, 2015, **448**, 17-23.
12. I. Sosnowska, T. P. Neumaier and E. Steichele, *Journal of Physics C: Solid State Physics*, 1982, **15**, 4835-4846.
13. K. F. Wang, J. M. Liu and Z. F. Ren, *Advances in Physics*, 2009, **58**, 321-448.
14. A. Filippetti and N. A. Hill, *Physical Review B*, 2002, **65**, 195120.
15. I. Levin, M. G. Tucker, H. Wu, V. Provenzano, C. L. Dennis, S. Karimi, T. Comyn, T. Stevenson, R. I. Smith and I. M. Reaney, *Chemistry of Materials*, 2011, **23**, 2166-2175.
16. N. Jeon, D. Rout, I. W. Kim and S.-J. L. Kang, *Applied Physics Letters*, 2011, **98**, 072901.
17. F. Gao, Y. Yuan, K. F. Wang, X. Y. Chen, F. Chen, J. M. Liu and Z. F. Ren, *Applied Physics Letters*, 2006, **89**, 102506.
18. J. Schiemer, R. L. Withers, M. A. Carpenter, Y. Liu, J. L. Wang, L. Noren, Q. Li and W. Hutchison, *Journal of physics. Condensed matter : an Institute of Physics journal*, 2012, **24**, 125901.
19. Q. Y. Xu, H. F. Zai, D. Wu, T. Qiu and M. X. Xu, *Applied Physics Letters*, 2009, **95**, 112510.
20. A. A. Belik, A. M. Abakumov, A. A. Tsirlin, J. Hadermann, J. Kim, G. Van Tendeloo and E. Takayama-Muromachi, *Chemistry of Materials*, 2011, **23**, 4505-4514.
21. X. W. Tang, J. M. Dai, X. B. Zhu and Y. P. Sun, *Journal of Alloys and Compounds*, 2013, **552**, 186-189.

22. W. Gao, W. Y. Xing, Q. Yun, J. Y. Chen, C. H. Nie and S. F. Zhao, *Journal of Materials Science: Materials in Electronics*, 2014, **26**, 2127-2133.
23. V. Koval, I. Skorvanek, M. Reece, L. Mitoseriu and H. Yan, *Journal of the European Ceramic Society*, 2014, **34**, 641-651.
24. D. H. Kim, H. N. Lee, M. D. Biegalski and H. M. Christen, *Applied Physics Letters*, 2007, **91**.
25. B. C. Luo, C. L. Chen, Z. Xu and Q. Xie, *Physics Letters A*, 2010, **374**, 4265-4268.
26. S. Godara, N. Sinha and B. Kumar, *Materials Letters*, 2014, **136**, 441-444.
27. X. M. Sun and Y. D. Li, *Angewandte Chemie International Edition*, 2004, **43**, 597-601.
28. W. W. Mao, X. W. Wang, Y. M. Han, X. A. Li, Y. T. Li, Y. F. Wang, Y. W. Ma, X. M. Feng, T. Yang, J. P. Yang and W. Huang, *Journal of Alloys and Compounds*, 2014, **584**, 520-523.
29. V. A. Khomchenko, D. V. Karpinsky, A. L. Kholkin, N. A. Sobolev, G. N. Kakazei, J. P. Araujo, I. O. Troyanchuk, B. F. O. Costa and J. A. Paixão, *Journal of Applied Physics*, 2010, **108**, 074109.
30. G. H. Dong, G. Q. Tan, W. L. Liu, A. Xia and H. J. Ren, *Ceramics International*, 2014, **40**, 1919-1925.
31. P. Godara, A. Agarwal, N. Ahlawat, S. Sanghi and R. Dahiya, *Journal of Alloys and Compounds*, 2014, **594**, 175-181.
32. Y. F. Cui, Y. G. Zhao, L. B. Luo, J. J. Yang, H. Chang, M. H. Zhu, D. Xie and T. L. Ren, *Applied Physics Letters*, 2010, **97**, 222904.
33. V. F. Freitas, L. F. Cótica, I. A. Santos, D. Garcia and J. A. Eiras, *Journal of the European Ceramic Society*, 2011, **31**, 2965-2973.
34. T. Maity, S. Goswami, D. Bhattacharya and S. Roy, *Physical Review Letters*, 2013, **110**, 107201.
35. D. P. Dutta, C. Sudakar, P. S. V. Mocherla, B. P. Mandal, O. D. Jayakumar and A. K. Tyagi, *Materials Chemistry and Physics*, 2012, **135**, 998-1004.
36. D. P. Dutta, O. Jayakumar, A. Tyagi, K. Girija, C. Pillai and G. Sharma, *Nanoscale*, 2010, **2**, 1149-1154.
37. M. M. Shirolkar, R. Das, T. Maity, P. Poddar and S. K. Kulkarni, *The Journal of Physical Chemistry C*, 2012, **116**, 19503-19511.
38. T. J. Park, G. C. Papaefthymiou, A. J. Viescas, A. R. Moodenbaugh and S. S. Wong, *Nano letters*, 2007, **7**, 766-772.
39. L. Neel, *Comptes Rendus Hebdomadaires Des Seances De L Academie Des Sciences*, 1961, **252**, 4075-&.
40. D. Lebeugle, D. Colson, A. Forget, M. Viret, A. Bataille and A. Gukasov, *Physical review letters*, 2008, **100**, 227602.
41. G. Catalan and J. F. Scott, *Advanced materials*, 2009, **21**, 2463-2485.
42. W. W. Mao, X. A. Li, Y. T. Li, X. W. Wang, Y. F. Wang, Y. W. Ma, X. M. Feng, T. Yang and J. P. Yang, *Materials Letters*, 2013, **97**, 56-58.
43. C. D. Hu, *Physical Review B*, 2008, **77**.
44. R. Das, G. Gopal Khan and K. Mandal, *Journal of Applied Physics*, 2012, **111**, 104115.
45. N. H. Hong, N. Thu Huong, T. Y. Kim, S. Goumri-Said and M. B. Kanoun, *The Journal of Physical Chemistry C*, 2015, **119**, 14351-14357.
46. D. Kothari, V. Raghavendra Reddy, A. Gupta, C. Meneghini and G. Aquilanti, *Journal of physics. Condensed matter : an Institute of Physics journal*, 2010, **22**, 356001.
47. D. P. Dutta, B. P. Mandal, R. Naik, G. Lawes and A. K. Tyagi, *The Journal of Physical Chemistry C*, 2013, **117**, 2382-2389.
48. X. Qi, J. Dho, R. Tomov, M. G. Blamire and J. L. MacManus-Driscoll, *Applied Physics Letters*, 2005, **86**, 2903.
49. S. W. Cheong and M. Mostovoy, *Nature materials*, 2007, **6**, 13-20.
50. H. M. Christen, J. H. Nam, H. S. Kim, A. J. Hatt and N. A. Spaldin, *Physical Review B*, 2011, **83**, 144107.